14th International Symposium on Turbulence and Shear Flow Phenomena (TSFP14)
Heidelberg, Germany, July 28–31, 2026

NUMERICAL SIMULATION OF FLOW IN KARST CONDUITS

Ismail El Mellas
Spanish National Research Council (IDAEA-CSIC)
C. Jordi Girona 18-26,
08034 Barcelona, Spain
ismail.elmellas@idaea.csic.es

Alexander Stroh
Institute of Fluid Mechanics (ISTM)
Karlsruhe Institute of Technology (KIT)
Kaiserstr. 10, 76131 Karlsruhe, Germany
alexander.stroh@kit.edu

Juan J. Hidalgo
Spanish National Research Council (IDAEA-CSIC)
C. Jordi Girona 18-26,
08034 Barcelona, Spain
juanj.hidalgo@idaea.csic.es

Marco Dentz
Spanish National Research Council (IDAEA-CSIC)
C. Jordi Girona 18-26,
08034 Barcelona, Spain
marco.dentz@idaea.csic.es

ABSTRACT

Karst conduits exhibit strong geometric irregularities that control flow resistance and transport but are often represented by smooth-pipe models. High-fidelity simulations with Nek5000 show that such irregularities act as effective roughness elements, increasing drag, promoting early transition, and producing coexisting laminar, transitional, and turbulent regions. A centreline-based framework is introduced to define hydraulic diameter and roughness, providing global descriptors suitable for simplified network-scale models of karst aquifers.

FLOW AND TRANSPORT IN KARST CONDUITS

Most conduits, whether natural or engineered, deviate from being straight and smooth. Variations in cross-section, curvature, and wall topography strongly affect flow resistance and mixing, yet hydrological models often rely on empirical relations derived for smooth pipes, such as the Hagen-Poiseuille law or the Darcy-Weisbach equation (Cohen & Kundu, 2004), where wall roughness is either neglected or assumed to be very small. Karst caves offer a clear natural demonstration: dissolution of bedrock by freshwater creates channels with highly irregular geometries and rough walls (Dreybrodt, 2012), where wall variations may represent a significant fraction of the conduit radius (Curl, 1966; Claudin *et al.*, 2017). This work examines flow behaviour in karst conduits by combining idealised and natural geometries to identify key geometrical and fluid mechanical parameters. Wavy channels are often employed as representative conduits, since their variable cross-section and pronounced wall roughness capture essential features of karst, while simulations of real cave geometries extend the analysis to the irregularity of natural systems. Parameters such as average cross-sectional area, conduit centreline, friction factor, and velocity distribution are evaluated through direct numerical simulations across a wide range of flow conditions, enabling a systematic assessment of how geometry and roughness influence resistance and transport. These variables provide global characteristics that can be used to represent conduits in simplified forms, for instance within graph-based network models, which avoid the need to resolve every conduit in detail. This connection is particularly important given that karst aquifers, with their extensive and intricate conduit networks, play a central role in groundwater flow and contaminant transport (Parise & Gunn, 2007).

METHODS

Geometry definition

Two types of geometries were considered. The first consists of idealised wavy pipes defined analytically to reproduce controlled cross-sectional variations representative of large-scale confinements. The second consists of natural karst conduits reconstructed from in situ LiDAR scans. The LiDAR point clouds were processed into continuous triangulated surfaces suitable for numerical simulation, while preserving the morphological features of the caves.

All simulations were performed with the high-order spectral element solver Nek5000 (Fischer *et al.*, 2008). The flow was driven by prescribing the bulk velocity $u_b = \frac{1}{V}\int_\Omega u dV$, from which the Reynolds number was defined as $\mathrm{Re} = u_b D/\nu$, where D is the reference pipe diameter and ν the kinematic viscosity. Periodic boundary conditions were used for the reference cases. These include a smooth pipe representing the reference case and a wavy pipe capturing controlled roughness, as introduced in the validation of the numerical framework section. Both cases admit periodic boundary conditions due to their axisymmetry.In contrast, for the natural karst conduit, pressure was fixed at the outlet due to the non-periodic nature of the geometry.

IBM and ray tracing

To handle complex cave geometries without body-fitted meshing, an immersed boundary method (IBM) (Fadlun *et al.*, 2000) coupled with ray tracing was implemented in Nek5000. The geometry surface, represented as a triangulated STL mesh, is intersected locally with spectral elements to classify grid points as fluid or solid with a classification function $\chi(\mathbf{x})$. No-slip conditions are imposed at the immersed boundary through a forcing term in the momentum equation:

$$\mathbf{f}_{\rm IBM} = -\alpha\,\chi(\mathbf{x})\,\mathbf{u} - \beta\,\chi(\mathbf{x})\,\mathbf{u}_{\rm int}, \tag{1}$$

where α and β are penalisation coefficients controlling the instantaneous and integral damping, respectively, and $\mathbf{u}_{\rm int}$ is an auxiliary field that accumulates the local velocity in time according to

$$\mathbf{u}_{\rm int}^{n+1} = \mathbf{u}_{\rm int}^{n} + \mathbf{u}^{n}\,\Delta t. \tag{2}$$

This approach combines the high-order spectral element solver of Nek5000 with an immersed-boundary representation, avoiding the cost and potential instability of generating conformal meshes for highly irregular geometries.

Centreline extraction

Defining a characteristic diameter in natural conduits is a non-trivial task since the conduit axis is not necessarily straight and the cross-section may vary in both size and shape along the flow direction. Irregular boundaries, bends, contractions, and expansions make the identification of a representative length scale significantly more challenging than in ideal circular pipes. A first step is therefore the definition of a meaningful centreline along which the local geometry can be analysed.

In this work, two approaches were considered to identify the centreline. The first was a geometric centreline extracted directly from the conduit surface. The surface point cloud was sliced along the main direction, the cross-section of each slice was reconstructed, and the centroid of area was computed. Connecting these centroids produced a smooth axis purely based on the conduit morphology of length L_c.

The second approach was a hydraulic centreline obtained from particle tracking in the creeping-flow limit. Massless tracers were transported by pure advection using a Langevin-type equation without inertia,

$$\frac{d\mathbf{x}}{dt} = \mathbf{u}(\mathbf{x},t), \tag{3}$$

so that particle motion followed the local velocity field. Particles were seeded over the entire inlet cross-section using a flux-weighted distribution based on the local normal velocity. For the conduit considered here, the imposed inlet boundary condition yields an approximately uniform inlet velocity profile, so the flux-weighted procedure is effectively equivalent to uniform seeding over the inlet plane. The streamwise evolution of the centre of mass of the particle cloud defined the hydraulic centreline.

Both definitions gave very similar results, with only small deviations observed in strongly curved regions of the conduit. For the present work, the hydraulic centreline was adopted. The geometric approach is simpler and cheaper to extract, whereas the hydraulic definition requires an additional flow simulation but can provide a more accurate reference axis in highly complex geometries.

Cave decomposition

Surface roughness exhibits multiscale characteristics that affect hydraulic resistance and cannot be described by a single length scale alone (Flack & Schultz, 2010). To quantify geometric variability and enable a scale-based decomposition of wall deviations, the conduit geometry is referenced to an equivalent circular pipe representation. This reference geometry is centred on the hydraulic centreline and assigned a constant radius, R_{ref}, defined as the mean radius of the original conduit over the analysed domain. For each streamwise location x and azimuthal angle θ, a local radius $R(x,\theta)$ is computed from the cave surface and compared to the reference radius R_{ref}. Based on this comparison, a non-dimensional roughness field is defined as

$$\frac{k(x,\theta)}{R_{\rm ref}} = \frac{R_{\rm ref} - R(x,\theta)}{R_{\rm ref}}. \tag{4}$$

This formulation provides a direct connection with classical pipe-flow concepts, while recognising that natural conduit cross-sections can deviate substantially from an ideal circular shape. Further, the field $k(x,\theta)$ was decomposed into contributions from different geometric scales. First, the largest-scale contribution related to centreline tortuosity was isolated by reconstructing a baseline conduit with a smooth circular constant radius (R_{ref}) mapped along the tortuous centreline. The remaining cross-sectional variability was then split into an intermediate (large-scale) component and a residual (small-scale) component by applying a Fourier-based filter in θ at each x. Specifically, the circumferential spectrum was decomposed using an energy-based low-pass filter. The lowest wavenumber modes were retained such that 98% of the cross-sectional variance was preserved, defining the large-scale component, while the remaining high-wavenumber content was assigned to the small-scale residual roughness. This cutoff was adopted as a fixed operational choice for the present analysis to provide a consistent scale decomposition across all cases. Both components were regularised to remove outliers and ensure smooth reconstruction. Finally, three idealised conduits were generated from these fields: (i) a tortuous baseline pipe with circular cross-sections, (ii) a straight pipe retaining only the large-scale cross-sectional modulation, and (iii) a straight pipe retaining only the small-scale residual roughness. All reconstructed surfaces were exported as STL meshes for subsequent immersed boundary simulations, enabling the hydraulic impact of each geometric scale to be assessed separately.

Average statistics

For each conduit, cross-sectional statistics were obtained from a set of planes normal to the centreline and expressed in a local (y,z) frame. To enable averaging across multiple sections, cell-centred data were mapped onto a common uniform grid using bilinear interpolation with area-weighted projection, ensuring a consistent area-weighted mapping between the slice discretisation and the structured grid. All statistics were then volume-weighted, with weights proportional to the cell volume divided by the local slice spacing, ensuring consistency with a three-dimensional volume integral over the conduit. Velocity components were also expressed in cylindrical form, computed from the in-plane Cartesian velocities relative to the slice origin, giving axial, radial, and azimuthal components. In addition to averages over the full cross-section, separate statistics were computed in prescribed radial regions to distinguish core and near-wall behaviour. Because the conduit geometry is irregular, a unique radial coordinate is not available. Instead, a wall-distance field was computed on the common grid using a Euclidean distance transform of the fluid–solid mask. This provides, at each fluid location, the shortest distance to the wall and therefore a generalised wall-normal coordinate for arbitrary cross-sectional shapes.

Mean velocity profiles were then constructed by averaging the regridded fields as a function of wall distance. Because the flow is non-periodic and spatially developing, a single representative friction velocity was defined from the global pressure drop as

$$u_\tau = \sqrt{\frac{R\Delta p}{2L_c\rho}}, \tag{5}$$

where Δp is the pressure drop along the cave with centreline length L_c and ρ is the fluid density. Using the friction friction velocity, the profiles were expressed in inner variables as

$$U^+ = \frac{U}{u_\tau}, \qquad y^+ = \frac{y u_\tau}{\nu}, \tag{6}$$

thereby providing a direct analogue of the classical U^+ - y^+ representation for complex conduits. Because the simulations are not periodic in the streamwise direction, statistics were computed both over the full domain and over a truncated region excluding the inlet development length.

RESULTS

Canonical Geometries

To assess the accuracy of the numerical framework, simulations were first performed for turbulent flow in a smooth pipe at $Re_\tau = 180$. The inner-scaled mean velocity profile $U^+(y^+)$ together with velocity fluctuations and Reynolds shear stress, are shown in Fig. 1a,b. The results are in close agreement with reference DNS data from Pirozzoli *et al.* (2021). The same methodology was then applied to the wavy pipe configuration. The geometry was defined through a sinusoidal modulation of the radius,

$$R(z) = R_{\max} - \frac{k}{2}\left[1 - \sin\left(\frac{2\pi z}{\lambda}\right)\right], \tag{7}$$

where $k = R_{\max} - R_{\min}$ is the wall amplitude and λ the streamwise wavelength. In this study, the amplitude was varied while the wavelength was kept fixed. This design produces strong cross-sectional variations, with constrictions reducing the local radius by up to 40%, and serves as a simplified model for karst conduits with large-scale roughness. For brevity only a case here is reported with the strongest modulation $\overline{R}/k = 2$ and $Re_\tau = 125$. Figure 1c,d reports inner-scaled mean velocity profiles and turbulence statistics for the wavy pipe with. Results obtained with the present immersed boundary approach show very good agreement with previous simulations performed using a body-fitted mesh (El Mellas *et al.*, 2025), confirming the consistency of the two numerical strategies. Direct numerical simulations reveal that wall waviness strongly modifies flow behaviour across regimes. Inner-scaled mean velocity profiles exhibit a clear downward shift, with a roughness function ΔU^+ of 8–10 for this geometry. Such values are typical of fully rough turbulent pipe flow (Jiménez, 2004), highlighting the strong drag penalty imposed by large-scale waviness. Results show that once a critical roughness threshold is exceeded, flow reversal appears at low Reynolds numbers, inducing local recirculation zones, in the diverging sections. Between the laminar and fully rough turbulent regimes, the flow exhibits a transitional state governed by finite-amplitude effects, that follows an approximate power-law scaling between wall amplitude and Reynolds. Overall, large-scale wall modulation acts as an effective roughness that increases drag and destabilises laminar flow.

Real Cave Geometry

To assess flow in realistic karst conduits, the Faux-Monnayeurs cave, located in France, was analysed as a representative case (Fig. 2a). The conduit centrelines obtained from the geometrical and hydraulic evaluation are both reported in the figure. The cave exhibits pronounced geometric complexity, with irregular cross-sections varying along a tortuous path, making it an ideal candidate for investigating the hydraulic consequences of natural conduit morphology.

The importance of geometry is further highlighted by the roughness analysis map reported in Fig. 2b. This map reveals strong heterogeneity both along the axis and around the perimeter, reflecting deviations from the circular reference cross-section toward more elliptical or square-like forms. To systematically isolate the hydraulic effects of different geometric features, we adopt a scale-separation framework: (i) the largest scale, associated with tortuosity and global centreline curvature, is first removed by referencing the conduit to a circular pipe; (ii) an intermediate scale, capturing systematic cross-sectional modulation and large obstacles (e.g., rocks, sinkholes), can subsequently be extracted through spectral filtering; (iii) while finer wall irregularities remain as residual roughness. The resulting reconstructions span a range of roughness values: the original cave and large-scale geometry share $\overline{R}/k \approx 5$, the small-scale geometry yields $\overline{R}/k \approx 45$, and the tortuous reconstruction (with cross-section kept constant) corresponds to $\overline{R}/k \to \infty$ (hydraulically smooth). Although only the first decomposition step is presented here, this multi-scale approach enables the reconstruction of idealised conduits retaining individual roughness components separately, by that allowing quantification of their respective hydraulic contributions.

To investigate the individual contributions of each roughness component, numerical simulations were performed on the four distinct geometries: the original cave and three reconstructions derived from the scale-separation procedure. All simulations were conducted at constant bulk velocity u_b, with Reynolds numbers spanning from creeping flow to fully turbulent regimes. Figure 3 presents results for $Re = 1000$, where panel (a) shows the cross-sectionally averaged pressure variation $p(x)$ along the centreline x. The large-scale roughness exhibits the dominant influence: while the small-scale and tortuosity-only profiles appear nearly linear, the large-scale reconstruction displays pronounced pressure fluctuations that closely track the original cave data, reflecting the strong cross-sectional variations along the conduit. This morphological complexity leads to a coexistence of laminar regions, turbulent patches, and transitional states within the conduit. Such organisation complicates direct comparison with canonical pipe flows, since bends and asymmetries distort the velocity field and can even alter the orientation of the main flow component, preventing the development of a uniform equilibrium profile. The influence of wall irregularities is directly reflected in the friction factor, evaluated according to the Darcy-Weisbach equation $f = 2D\Delta p/(L_c\rho u_b^2)$ (White, 2011). The cave data deviate strongly from smooth-pipe predictions and instead align more closely with the behaviour observed in wavy geometries, even in the laminar regime where the Poiseuille law fails. This discrepancy arises because the average diameter overestimates the effective cross-sectional area available to the flow. To account for these geometric effects, we introduce an effective hydraulic radius $R_h = \sqrt{8\mu u_b L_c/\Delta p}$ obtained from the laminar simulations. It is defined in the spirit of an effective conductance as the radius of an equivalent straight pipe that has the same laminar flow resistance as the cave conduit. Velocity profiles are reported in Fig. 3b in wall units. For reference, the figure includes profiles from a smooth pipe at comparable friction Reynolds number and a wavy pipe simulation with equivalent roughness ($\overline{R}/k = 5$) from previous studies. Complementary two-dimensional contour views of the mean streamwise velocity field u_x in the axial plane are provided in Fig. 3c for qualitative visualisation of the flow structure. The original geometry exhibits strong velocity variations and extensive flow reversal near irregular wall bulges, reflecting the combined influence of all roughness scales. The tortuous geometry shows a much smoother field with gentle curvature-driven redistribution but little separation. The small-scale geometry appears nearly uniform with minimal streamwise variation, consistent with its weak hydraulic impact. The large-scale geometry displays pronounced modulation with isolated recirculation zones at severe constrictions, yet maintains a more organized structure than the original cave, due to the absence of the tortuosity. These profiles confirm that large-scale modulation dominates the flow distortion, while small-scale roughness and pure tortuosity produce relatively mild effects. This suggests that the essential hydraulic behaviour of complex natural conduits may be captured by retaining only the large-scale geometric features, a finding with significant implications for predictive modelling in karst systems. The results mirror the pressure field trends: small-scale and tortuous geometries exhibit laminar-like behaviour. The small-scale profile appears flattened toward the centre, explained by the limited roughness influence (consistent with the linear pressure drop) combined with insufficient streamwise length to reach fully developed conditions, a consequence of the non-periodic domain. Conversely, the tortuous geometry displays a more developed parabolic profile, attributed to flow curvature redistributing momentum and accelerating development.

The original cave and large-scale reconstruction, however, show profiles resembling turbulent rough-pipe flow, comparable to the wavy pipe reference. The near-wall region appears nearly constant and close to zero, attributable to extreme geometric complexity creating zones of flow reversal or stagnation. Inner-scaled mean velocity profiles exhibit a clear downward shift, with a roughness function $\Delta U^+ \approx 10$–12, typical of fully rough turbulent regimes.

It should be noted that this representation follows conventional pipe-flow methodology for comparison purposes, yet its applicability is limited here. The averaging combines cross-sections of varying shape and area along a non-straight centreline, while the wall-distance field, computed via Euclidean distance transform from the binary occupancy map, becomes ambiguous where the local geometry deviates substantially from circular. Thus, the profiles serve primarily as a qualitative diagnostic rather than a rigorous similarity variable.

SUMMARY AND OUTLOOK

In conclusion, classical characterisations of flow in rough conduits based on the Moody diagram and analytical correlations for the Darcy-Weisbach friction factor need to be reassessed for conduits with strong wall modulations (Flack, 2018). This requires revisiting fundamental definitions: the effective hydraulic diameter in laminar regimes, sandgrain roughness in turbulent regimes, and the boundaries between these regimes must be connected to predictable geometric properties rather than empirical fits.

The present results demonstrate that strong cross-sectional variability acts as effective roughness, enhancing friction, shifting velocity profiles, and promoting early transition. Wavy channels successfully reproduce key signatures of rough-wall behaviour, while analysis of the Faux-Monnayeurs cave confirms that natural conduits exhibit multi-scale roughness and mixed flow regimes. Crucially, scale-separation analysis reveals that large-scale modulation dominates hydraulic resistance and velocity distribution, while small-scale roughness and centreline tortuosity contribute secondary effects. This implies that simplified geometric representations retaining only intermediate-scale features may suffice for predictive modelling, substantially reducing computational cost while preserving essential flow physics. Defining global descriptors relative to the conduit centreline provides a consistent framework for comparison and a starting point for upscaling.

Future work should validate these findings across broader Reynolds number ranges and conduit morphologies to establish general criteria for geometric simplification in karst hydrology applications, and address how different roughness scales can be represented through simplified models and tested across diverse cave systems.

ACKNOWLEDGMENTS

This project has received funding from the European Research Council (ERC) under the European Union's Horizon Europe research and innovation programme (grant agreement No. 101071836, KARST)

REFERENCES

Claudin, P., Durán, O. & Andreotti, B. 2017 Dissolution instability and roughening transition. *J. Fluid Mech.* **832**, R2.

Cohen, I. M. & Kundu, P. K. 2004 *Fluid Mechanics*. Elsevier.

Curl, R. L. 1966 Caves as a measure of karst. *J. Geol.* **74** (5, Part 2), 798–830.

Dreybrodt, W. 2012 *Processes in Karst Systems: Physics, Chemistry, and Geology*, , vol. 4. Springer.

El Mellas, I., Hidalgo, J. J. & Dentz, M. 2025 Laminar and turbulent flow in wavy pipes under strong wall modulations. *arXiv preprint arXiv:2511.17458* .

Fadlun, E. A., Verzicco, R., Orlandi, P. & Mohd-Yusof, J. 2000 Combined immersed-boundary finite-difference methods for three-dimensional complex flow simulations. *J. Comput. Phys.* **161**, 35–60.

Fischer, P. F., Lottes, J. W. & Kerkemeier, S. G. 2008 Nek5000. `http://nek5000.mcs.anl.gov`.

Flack, Karen A 2018 Moving beyond moody. *Journal of Fluid Mechanics* **842**, 1–4.

Flack, K. A. & Schultz, M. P. 2010 Review of hydraulic roughness scales in the fully rough regime. *J. Fluids Eng.* **132** (4), 041203.

Jiménez, J. 2004 Turbulent flows over rough walls. *Annu. Rev. Fluid Mech.* **36**, 136–196.

Parise, M. & Gunn, J. 2007 Natural and anthropogenic hazards in karst areas: an introduction. *Geol. Soc. Lond. Spec. Publ.* **279**, 1–3.

Pirozzoli, P., Romero, S., Fatica, M., Verzicco, R. & Orlandi, P. 2021 One-point statistics for turbulent pipe flow up to $Re_\tau \approx 6000$. *J. Fluid Mech.* **926**, A28.

White, F. M. 2011 *Fluid Mechanics*, 7th edn. McGraw-Hill.

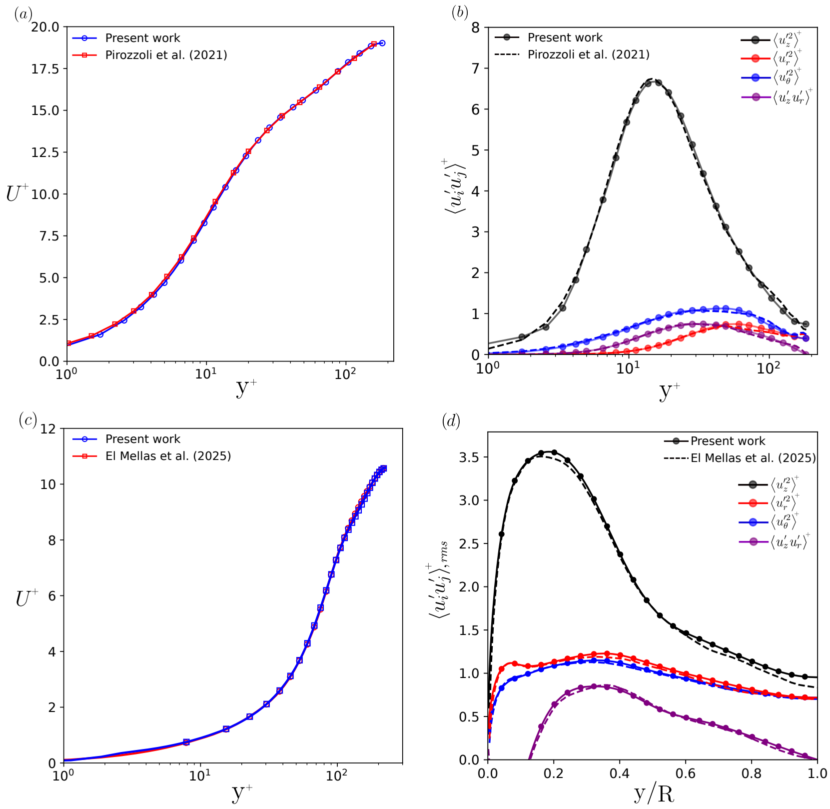

Figure 1: Validation of the immersed-boundary method (IBM) using two benchmark cases. (a,b) Smooth pipe flow at $Re_\tau = 180$: (a) mean velocity profile in wall units (U^+ vs. y^+) and (b) Reynolds stress components normalised by the friction velocity squared (u_τ^2), including the velocity variances $\langle {u'_r}^2 \rangle^+$, $\langle {u'_\theta}^2 \rangle^+$, $\langle {u'_z}^2 \rangle^+$, and the Reynolds shear stress $\langle u'_r u'_z \rangle^+$. Results are compared with the reference data of Pirozzoli *et al.* (2021). (c,d) Wavy pipe flow for $\overline{R}/k = 2$ at $Re_\tau = 120$: (c) mean velocity profile in wall units and (d) Reynolds stress components normalised by u_τ^2. Results are compared with a previous body-fitted mesh simulation El Mellas *et al.* (2025). Filled markers denote the present IBM simulation, and dashed lines indicate the reference data.

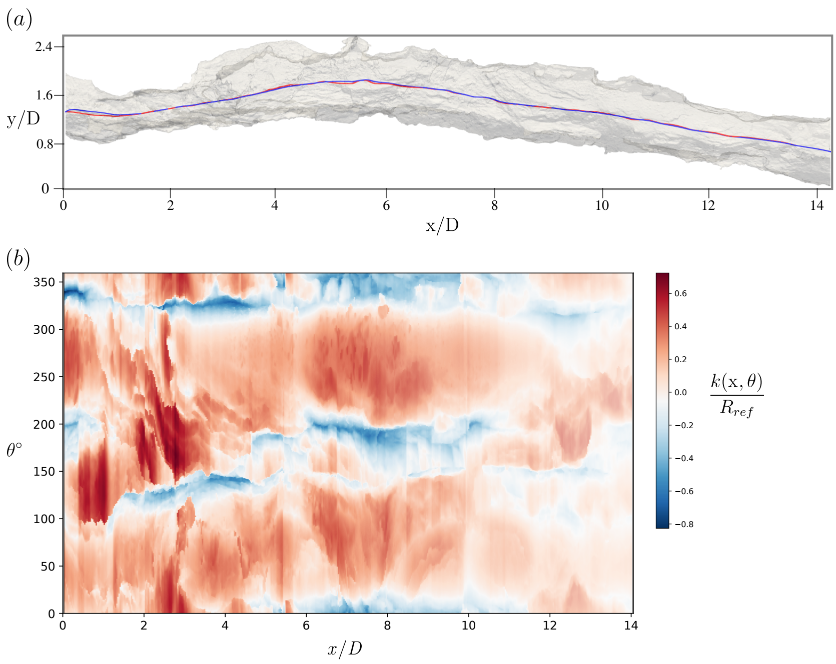

Figure 2: Real cave study results: FauxMonnayeur cave (France). (a) Top view of the cave geometry. The centrelines obtained from the geometric method and from particle tracking are shown by the red and blue lines, respectively. (b) Non-dimensional roughness map, $k(x,\theta)/R_{\text{ref}}$, showing local wall deviations from an equivalent reference circular conduit of radius R_{ref} defined from the mean cross-sectional area.

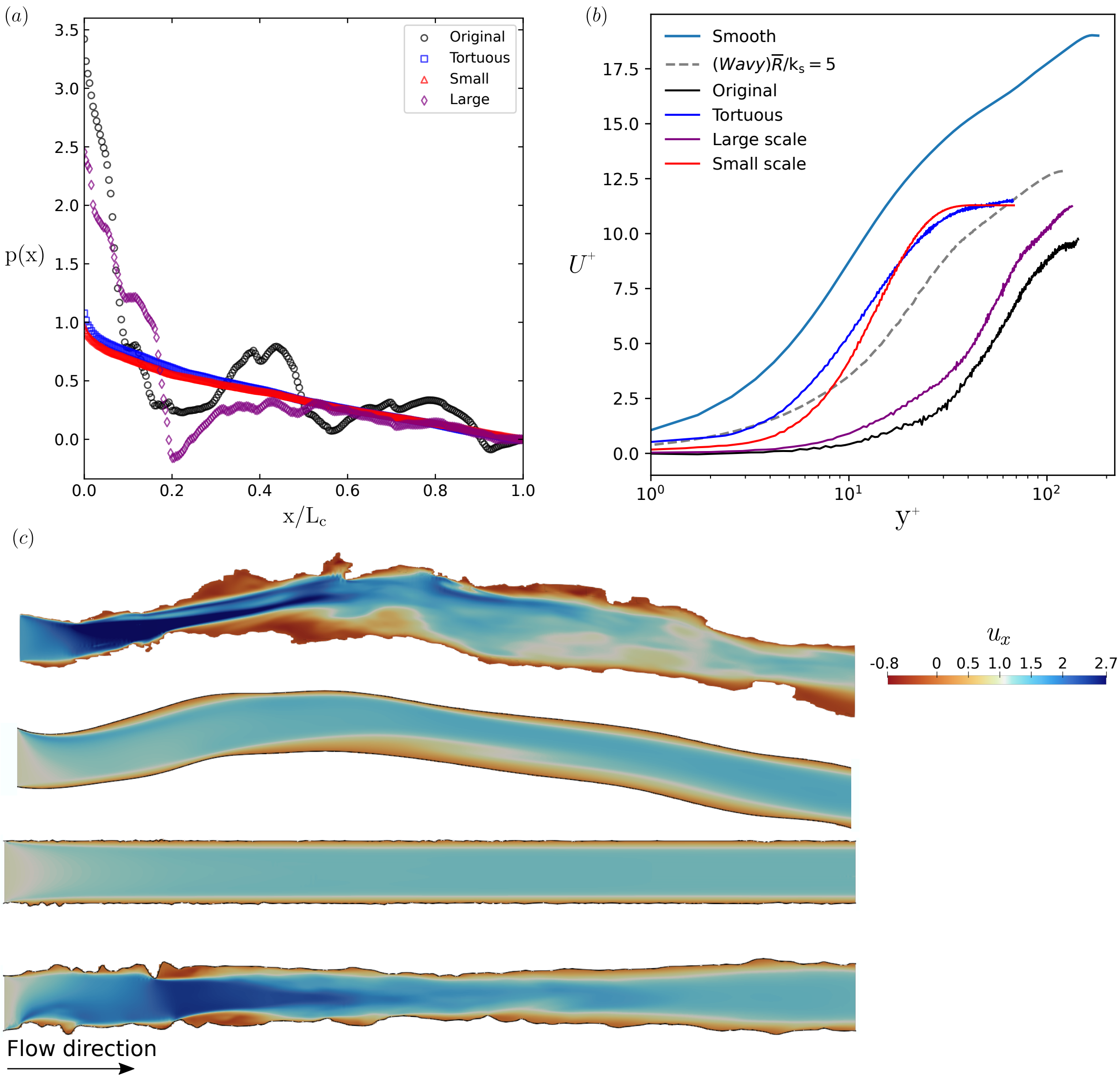

Figure 3: Real cave study results: effect of different roughness scales at $Re = 1000$. (a) Cross-sectionally averaged pressure, $p(x)$, along the centreline coordinate, x. (b) Mean velocity profiles in wall units (U^+ vs. y^+) for the different geometries. For reference, the profiles of a smooth pipe with comparable friction Reynolds number and of a wavy pipe with $\overline{R}/k = 5$ at $Re_\tau = 120$ are also shown. (c) Two-dimensional contour views of the mean streamwise velocity field, u_x, extracted in the axial plane along the centreline for the four geometries. From top to bottom: original geometry, tortuous geometry, small-scale roughness, and large-scale roughness.